Optical-dipole-force fiber guiding and heating of atoms

Michael J. Renn,* Alex A. Zozulya, Elizabeth A. Donley, Eric A. Cornell,† and Dana Z. Anderson
JILA‡ and Department of Physics, University of Colorado, Boulder, Colorado 80309-0440
(Received 19 August 1996)

We present an experimental and theoretical investigation characterizing the flux of laser-guided atoms through hollow-core optical fibers and show how it depends on laser detuning from resonance, laser intensity, and fiber curvature. The guiding employs dipole forces arising from the interaction of the atoms with the optical field. Laser light is focused into the hollow region of 40-μm-inner-diam capillary fiber and guided through the fiber by grazing incidence reflection from the glass walls. The lowest-order mode is azimuthally symmetric with maximum intensity on the fiber axis and nearly zero intensity at the walls. Rubidium atoms are attracted to the high-intensity region along the axis when the laser is detuned to the red of resonance and consequently guided through the fiber. Of particular interest is the evolution of the atom-flux versus laser-detuning profile of increasing intensity. At low intensities the dipole guiding potential is purely conservative and the flux profile is roughly dispersion shaped. At high intensity, viscous dipole forces heat the atoms and ''burn a hole'' in the flux-detuning curve. We find that transverse heating of the atoms and the exponential attenuation of optical mode intensity limit the distance atoms may be guided to about 20 cm in a 40-μm-diam fiber. Bending the fiber can reduce the effects of heating on atom flux. [S1050-2947(97)04604-0]

PACS number(s): 42.50.Vk, 42.81.Qb, 32.80.Pj

I. INTRODUCTION

In recent work Renn and coworkers [1,2] and Ito *et al.* [3] demonstrated atom guiding through hollow core optical fibers. The atoms are kept away from the inner glass walls by light that is also guided in the fiber. The notion of guiding atoms in hollow fibers with light was first suggested by Ol'shanii, Ovchinnikov, and Letokhow [4], and was further elaborated on by Marksteiner *et al.* [5] Fiber-guided atoms may lead to an effective method for transporting cold atoms, for example, from one vacuum system to another. It is furthermore intriguing to consider the potential of fiber atom optics: The deBroglie wavelength of sufficiently cold atoms approaches the hollow diameter, in which circumstance atoms propagate in modes much like the optical modes of conventional optical fibers [5]. In this domain lies the possibility of Mach-Zehnder, Sagnac, and other interferometer configurations. It is our hope that the hollow core fiber may lead to a robust technology for atom interferometry and other cold atom experiments.

Atoms may be guided through hollow core fibers either by grazing incidence or evanescent light. The primary purpose of this work is to investigate in some detail the characteristics of grazing-incidence guiding. In this configuration, laser light is launched into the hollow region of a glass capillary fiber and guided by grazing-incidence reflection from the glass walls. The lowest-order grazing-incidence mode is azimuthally symmetric, and has a maximal intensity along the fiber axis [6–9]. With the laser tuned to the red of the atomic resonance, atoms are attracted to the high-intensity region along the axis, and guided through the fiber. Experiments using this method have shown that atoms may be guided around bends in curved fibers and sections of the fiber may be exposed to air: the glass wall is sufficient to maintain vacuum in the fiber [1]. We present an extended experimental and theoretical study of the grazing-incidence mechanism of atom guiding. Measurements and calculations are presented which characterize the dependence of guided atom flux on laser intensity, detuning from atomic resonance, and fiber radius of curvature. The most striking character is the dependence of the flux on detuning from resonance. At low intensities the dipole force is purely conservative, and leads to a guided flux spectrum that is roughly dispersion shaped and sharply peaked near zero detuning. At high intensities, however, a viscous component of the dipole force [10] heats the atoms, and causes an exponential attenuation of atom flux with distance along the fiber. This heating term ''burns a hole'' in the flux spectrum such that the guided atom flux is large at large detunings and has a dip at moderate detunings. We also show that the dipole heating force may be reduced relative to the guiding force simply by bending the fiber.

Grazing-incidence atom guiding is reasonably straightforward in practice for fibers having diameters much larger than the wavelength of the guiding light. However, it has limitations that probably make it impractical for atom interferometry applications. Grazing-incidence modes decay exponentially as they propagate along the fiber; for a fiber having a 40-μm hole diameter, the fundamental grazing incidence modes has a $1/e$ attenuation length of $\sim$3.1 cm. The attenuation limits the useful length of a fiber, and since the attenuation length varies as the cube of the hole diameter, it also

*Permanent address, Physics Department, Michigan Technological University, Houghton, MI 49931.

†Staff member, Quantum Physics Division, National Institute of Standards and Technology, Boulder, CO 80309.

‡JILA is a joint institute of the National Institute of Standards and Technology and the University of Colorado.

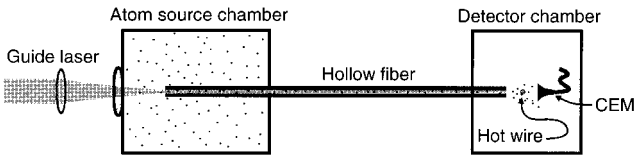

FIG. 1. Experimental apparatus. A hollow core fiber joins two vacuum chambers, one serving as the source of rubidium atoms, the other housing an atom detection apparatus consisting of an ionizing rhenium hot wire and a channeltron electron multiplier (CEM).

sets practical limits on the hollow diameter. Dipole heating combined with the exponential decay of optical intensity limits the distances over which atoms may be guided by grazing-incidence optical modes to about 20 cm through a 40-μm-diam fiber.

The paper is structured as follows. In Sec. II, we provide a context for the remainder of the paper by describing the generic grazing-incidence guiding experiment, and in Sec. III we describe the salient qualitative features of the results. In Sec. IV we present a simple theoretical model which allows the flux through a fiber to be calculated. Closed-form solutions can be obtained in various limiting cases such as large detuning and small intensities. We derive general expressions showing the dependence of the atom flux on laser intensity, detuning from resonance, length of fiber, and fiber curvature. Finally, in Sec. V we compare numerical calculations with experimental measurements, and draw some concluding remarks in Sec. VI.

II. EXPERIMENTAL APPARATUS

The basic apparatus shown in Fig. 1 consists of two vacuum chambers connected by a glass capillary fiber having lengths ranging from 3 to 15 cm. The first vacuum chamber contains rubidium, and is heated to form a typical partial pressure of $\sim 10^{-6}$ Torr. Atoms near the entrance of the fiber with appropriate trajectories pass into the guide. When the atoms reemerge, they are ionized on a heated rhenium wire, and the ions are counted with a channeltron electron multiplier.

Light from either a free running diode laser or a standing-wave Ti:sapphire laser is coupled into the fiber through a window in the rubidium source chamber. Considerable attention is given to optimizing the optical coupling into the EH_{11} mode, which is the lowest-order, azimuthally symmetric, grazing-incidence mode. Like coupling light into a single-mode fiber, optimum coupling is achieved when the beam waist at the entrance of the fiber is approximately the size of the EH_{11} mode, and the axis of the fiber and beam coincide. For low-intensity high-resolution measurements, a 5-mW single-mode diode laser having a linewidth of $\sim$50 MHz

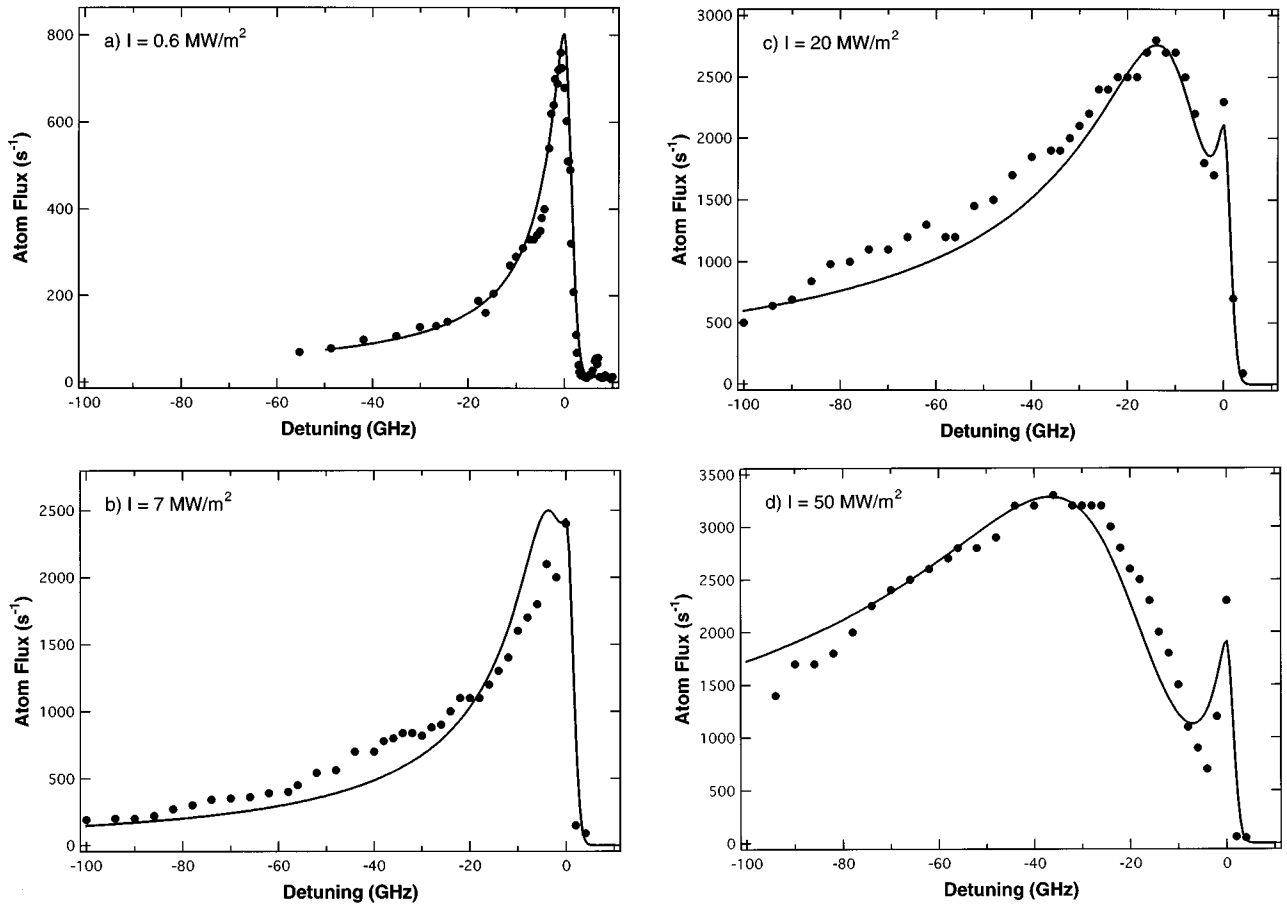

FIG. 2. Guided atom flux vs laser detuning from resonance at several laser intensities. The fiber lengths are 3.1 and 6.2 cm for (a) and (b)–(d), respectively, and the inner diameter is 40 μm. In Figs. 5(b) and 5(d) flux profiles with increasing titanium-sapphire laser intensity are shown. A spike near zero detuning is always observed due to the rapid turn off of the heating force relative to the guiding force as $\Delta \rightarrow 0$.

provides the guide light. Frequency tuning over a ±40-GHz range from resonance is accomplished by varying the injection current. A Ti:sapphire laser provides sufficient power to reach the high-intensity regime, up to 1 W, but operates on several longitudinal modes. The bandwidth of the Ti:sapphire laser is ≈2 GHz with an etalon in the cavity. The laser is tuned with the etalon over a range of ±60 GHz from resonance. Detuning from resonance is measured with an optical spectrum analyzer relative to the center of the $5S_{1/2}(F)-5P_{3/2}(F')$ hyperfine multiplet of rubidium.

III. QUALITATIVE RESULTS

In Fig. 2 we show the typical dependence of guided atom flux on detuning from resonance for several laser intensities. The experimental data are shown by points, the solid curves are theoretical fits to be discused later in the text. The profile of Fig. 2(a), representative of the low-intensity regime at $I_0=6\times10^5$ W/m^2, was measured using a low-power, single-mode diode laser. In Figs. 2(b) and 2(c), flux profiles with increasing titanium-sapphire laser intensity are shown. For all curves we observe the expected qualitative dependence: Atoms are guided when the laser is tuned to the red of resonance but not to the blue. At an intensity of ~0.6 MW/m^2 [Fig. 2(a)], the flux reaches a maximum near a detuning of about −1 GHz and then falls off rapidly for larger detunings. As we will show, this is expected from the conservative component of the dipole force. As the intensity is increased, as shown in Figs. 2(b)–2(d), a substantial flux is observed at significantly higher detunings. In addition, a dip forms in the flux profile at intermediate detunings. As a function of increasing intensity the dip grows deeper and broader [Figs. 2(c) and 2(d)]. We attribute the hole formation to viscous dipole forces which heat the atoms to larger transverse energies than can be guided.

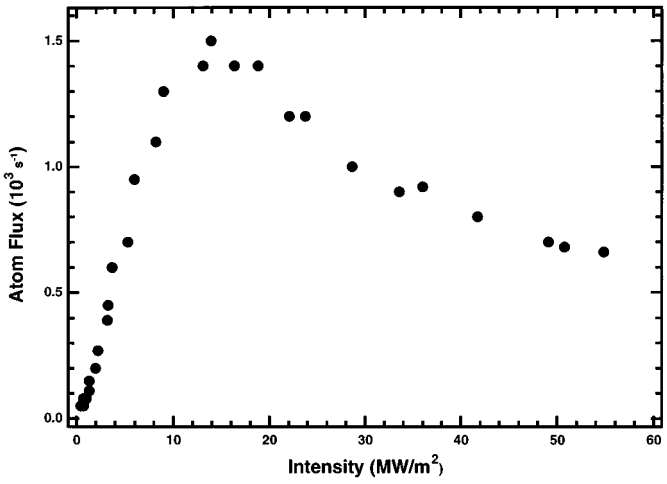

FIG. 3. Intensity dependence of the guided atom flux at $\Delta=-8$ GHz and a fiber length of 6.2 cm. At low intensity the flux increases linearly with intensity but at high intensity the flux decreases with increasing intensity. The high intensity decrease of flux is caused by the nonconservative component of the dipole force that heats the atoms.

The conservative and nonconservative characteristics of the dipole force are also evident in the intensity dependence of the flux. Figure 3 shows the intensity dependence for a detuning of −8 GHz from resonance. At low intensity, the flux increases linearly with intensity for all laser detunings from resonance, as expected in the limit of conservative dipole forces. However, at larger intensities the flux peaks and then decreases. Again, the flux decreases because the viscous component of the dipole force heats the atoms.

The formal treatment of atom guiding in the fiber, which is presented in the sections that follow, is rather involved. Yet it is not difficult to derive some insight into a qualitative understanding of the main features. At low guiding light intensities the guiding is described by the conservative dipole potential [10,11]

$$U=\frac{\hbar\Delta}{2}\ln\left(1+\frac{\omega_R^2}{2(\Delta^2+\Gamma^2)}\right), \tag{1}$$

where Δ is the laser frequency detuning from the atomic resonance, $\Delta=\omega_L-\omega_0$, Γ is the natural linewidth of the transition, and ω_R is the Rabi flopping frequency of the atom in the laser field,

$$\omega_R^2=\frac{2d^2I}{\hbar^2\varepsilon_0 c}, \tag{2}$$

I is the laser intensity and d is the dipole moment for the atomic transition, c is the speed of light, and ε_0 is the permittivity of free space. This potential arises from the dynamics Stark effect which shifts the atomic energy levels as illustrated in Fig. 4(a). As suggested by the figure, for red detuning of the laser the ground-state experiences an attractive force while the excited-state experiences a repulsive one.

When $\omega_R^2/\Delta^2\ll1$ the saturation effects are insignificant, and the atoms spend most of the time in the (attractive) ground state. An atom with sufficiently low initial transverse velocity simply oscillates back and forth in the concave bowl of the ground state as it propagates down the fiber. With the additional assumption $\Gamma\ll\Delta$, one can expand the logarithm in Eq. (1) in the low saturation limit to obtain a form that is linear in intensity and inversely proportional to the detuning. Figure 4(a) shows the intensity profile and level shifts when the laser is red detuned from an atomic resonance. The optical intensity profile in the fiber is maximum at the center of the hollow region, and falls to zero at the boundary. An atom predominantly in the ground state feels a force, $F_{\rm dip}=-\nabla U$, directed toward the center of the fiber.

Atoms moving in the high-intensity field experience viscous dipole forces which are directed parallel to the radial velocity, and heat the atoms for a red detuning from resonance. This force can be understood as a result of the time delay between absorption and emission of photons for a moving atom. Following Cohen-Tannoudji and Dalibard [10], we use the dressed-state atom-field picture to illustrate a case for which the energy of an atom is increased in its interaction with the optical field. The dressed picture for a two-level atom in a laser field, shown in Fig. 4(b), consists of a ladder of pairs of ground and excited state levels separated by the laser energy $\hbar\omega_L$. In the absence of coupling, the

states are labeled by the unperturbed atomic states g and e, and by the photon occupation number n. In this case the laser field is detuned to the red of the atomic transition, so the excited state lies above the ground state in each manifold pair. In the hollow region of the fiber where the light propagates, the atomic levels are mixed and energy shifted as they are in Fig. 4(a) by the dynamics Stark effect. The transverse confining of an atom in its ground state is seen to arise from the concave shape of the dressed-atom level; in the absence of spontaneous emission the atom simply oscillates back and forth in the inverted Gaussian bowl.

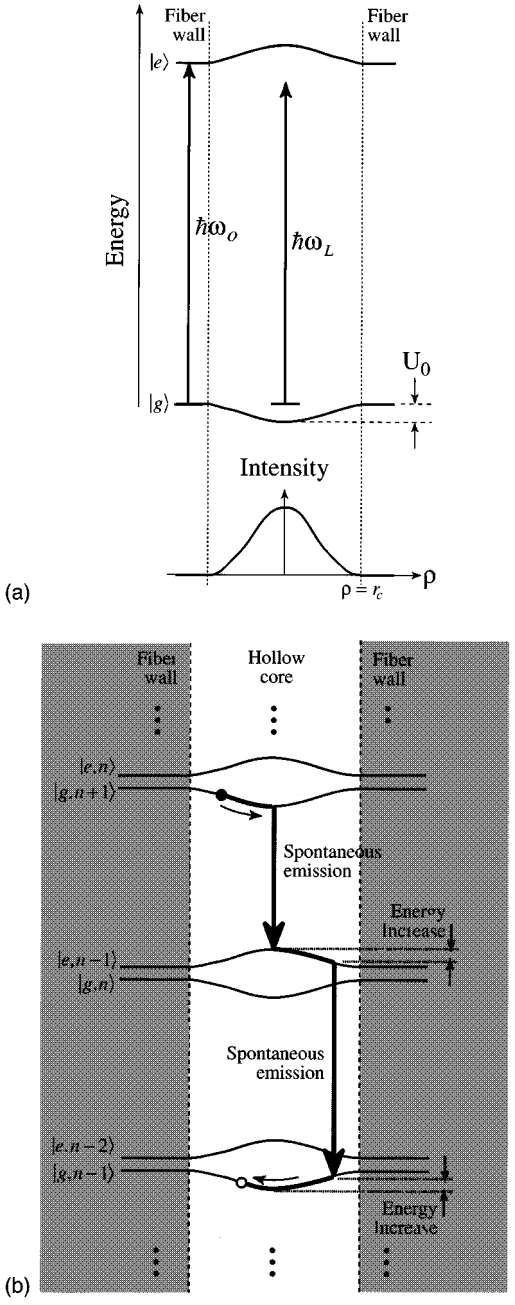

FIG. 4. (a) Spatial variation of the energy levels of a two-level atom interacting with a laser field of intensity $I(\rho)$ and frequency $\omega_L < \omega_0$. In the conservative limit of low intensities the atom remains in the ground state $|g\rangle$ and experiences a simple harmonic restoring force attracting it to $\rho=0$. (b) Dressed-state picture of the atom-field levels. At high intensity, the atom-field system has a significant probability to make a spontaneous transition to the repulsive state potential curve. The drawing illustrates the case in which the atom in the nominal excited state gains kinetic energy before decaying back to the nominal ground state and gains additional kinetic energy by the time it has completed a cycle.

Occasionally a spontaneous emission event can take the atom from its nominal ground state into its excited state; this is most likely to happen in the high-intensity region of the field where the unperturbed states are maximally mixed. Once it makes such a transition, the atom remains in the excited state on average for a lifetime $\tau_a = 2(\pi\Gamma)^{-1}$, and continues to move in the field. In the excited state the atom is now repelled by the field, and, as the figure illustrates, it gains kinetic energy as it rolls down the convex surface. Another spontaneous emission returns the atom to the nominal ground state. The second spontaneous event is most likely to occur in the low-intensity region near the walls, where the level mixing is minimum. In finishing its round trip, the atom rolls down the concave surface gaining additional kinetic energy. In the worst case pictured, the atom gains an energy equal to twice the optical potential depth (and escapes the confining field rather than make a complete round trip). The ensemble of atoms becomes heated through this cyclic process. It is this heating process that is responsible for the hole in the detuning dependence of atom flux shown in Fig. 2(d), as we shall discuss further in Sec. VI.

IV. THEORETICAL MODEL

In this section we develop the theoretical framework to calculate the guided atom flux through the fiber. The model takes into account three primary considerations. The first considers two components of the optical field, one giving rise to the (desirable) potential that guides the atoms and the other giving rise to the (undesirable) heating of the atoms as they propagate. The second consideration accounts for the Maxwell-Boltzmann distribution of the atomic velocities, and the fact that only a certain group of atoms within that distribution can be captured by the optical potential. The third consideration is that fact that the fiber may be curved, which changes the nature of the guiding characteristics somewhat.

In the following subsections we take these considerations into account in a progressive manner beginning with the general formalism in Sec. IV A. Section IV B analyzes the case of the straight fiber in the conservative force limit. Section IV C redoes the formalism to account for bending of the fiber. Section IV D includes the nonconservative portion of the atom-field interaction, and is used to predict the atom flux from a straight fiber at large intensities. We do not account for curved fibers in this last regime, as a proper treatment complicates the formalism substantially.

A. General equations

Accounting for both conservative and viscous dipole forces, the equations of motion for an atom of mass m in the fiber are given by [10]

$$\frac{d\mathbf{R}}{dt} = \boldsymbol{\nu}, \tag{3a}$$

$$m\frac{d\boldsymbol{\nu}}{dt}=-\frac{\hbar\Delta}{2}\frac{\omega_R^2 I}{\omega_R^2 I+2(\Delta)^2}\frac{\boldsymbol{\nabla} I}{I}-\frac{\hbar\Delta}{2\Gamma}\left[\frac{\omega_R^2 I}{\omega_R^2 I+2(\Delta)^2}\right]^3\left(\boldsymbol{\nu}\cdot\frac{\boldsymbol{\nabla} I}{I}\right)\frac{\boldsymbol{\nabla} I}{I}, \quad (3b)$$

where $\mathbf{R}=(X,Y,Z)$ is the atom's position in the fiber, $\Delta=\omega_L-\omega_0-k\nu_z$ is the laser detuning from resonance including the Doppler shift, k is the wave number of the laser light, and Z is the coordinate along the fiber. Here and in the remaining text, the Rabi frequency ω_R is taken at the intensity maximum. For ease of calculation, the intensity of the light $I(\mathbf{R})$ is normalized so that $I_{\max}=1$. The first term in the right-hand side of Eq. (3b) is the conservative dipole force term. The second term is the nonconservative viscous term that heats the atoms when the laser is tuned to the red of resonance ($\omega_L-\omega_0<0$) and cools them when tuned to the blue of resonance ($\omega_L-\omega_0>0$).

In the remainder of this section it is convenient to introduce the dimensionless coordinates $(x,y,z)=(X/r_c, Y/r_c, Z/l)$ and velocities $(u_x,u_y,u_z)=(\nu_x/\nu_\perp,\nu_y/\nu_\perp,\nu_z/\nu_T)$. The longitudinal coordinate Z is normalized to the length of the fiber l, and the transverse coordinates X and Y are normalized to the transverse hollow core radius r_c. The longitudinal velocity ν_z is normalized to the thermal velocity $\nu_T=\sqrt{2k_bT/m}$, where T is the temperature and k_b is Boltzmann's constant. The transverse velocities are normalized to the characteristic transverse velocity of a trapped atom $\nu_\perp=\sqrt{\hbar\omega_R/m}$, that is, the maximum transverse velocity allowed by the light-induced potential. Finally, a convenient dimensionless time τ is derived from the time τ_L it takes for a typical atom to traverse the length of the fiber: $\tau=t\nu_T/l$.

We assume that the longitudinal component $\partial I/\partial z$ of the intensity gradient ∇I in Eq. (3b) can be neglected compared to the transverse one. Equations (3) in the dimensionless variables can then be recast in the form

$$\frac{dz}{d\tau}=u_z, \quad (4a)$$

$$\frac{d\boldsymbol{\rho}_\perp}{d\tau}=a\mathbf{u}_\perp, \quad (4b)$$

$$\frac{d\mathbf{u}_\perp}{d\tau}=\frac{a\delta}{2}\left(\frac{I}{I+2\delta^2}\right)\frac{\boldsymbol{\nabla}_\perp I}{I}+\frac{b\delta}{2}\left(\frac{I}{I+2\delta^2}\right)^3\left(\mathbf{u}_\perp\cdot\frac{\boldsymbol{\nabla}_\perp I}{I}\right)\frac{\boldsymbol{\nabla}_\perp I}{I}, \quad (4c)$$

where $\boldsymbol{\rho}$ is the cylindrical coordinate radius vector, $a=l\nu_\perp/r_c\nu_T$ and $b=l\nu_\perp^2/\Gamma r_c^2\nu_T$, and $\boldsymbol{\nabla}_\perp$ is the transverse gradient operator. Finally, $\delta=-\Delta_n+su_z$ where $\Delta_n=\Delta/\omega_R$ is the normalized frequency detuning taken with a minus sign for convenience, and $s=k\nu_T/\omega_R$. The normalized time in Eq. (4) is within the range $0<\tau<l/u_z$. If the atom does not hit the wall by the time $\tau=1/u_z$ it passes through the fiber.

The relative importance of the velocity dependent nonconservative term in Eq. (4b) is determined by the value of the parameter b which can be written in terms of dimensioned times $b=(\tau_L/\tau_\perp)(\tau_a/\tau_\perp)$. The first factor is effectively the number of bounces a barely guided atom makes before it exits the fiber, and the second term is effectively the number of bounces the atom makes during one spontaneous decay lifetime. Thus, for relatively short (small τ_L) and/or wide (large $\tau_\perp$) fibers and moderate intensities (again large $\tau_\perp$), the contribution from the nonconservative term is small. In the next two subsections we calculate the fluxes working in the conservative limit so the second term in Eq. (4c) is dropped. In Sec. IV D, we include the nonconservative contribution to the force.

B. Conservative limit, straight fiber

In this section, we work in the conservative limit, and calculate the flux through a straight fiber. The nonconservative term in Eq. (4c) is neglected and the consequent equation is integrated, resulting in an energy conservation expression that is used to calculate the flux. Several assumptions can be made which greatly simplify the flux calculation. First, we assume that the distribution of atoms at the fiber input face is spatially uniform and has a Maxwell-Boltzmann velocity distribution. This assumption ignores the fact that atoms can be funneled into the fiber by the laser light. In addition, we use a parabolic and a square box intensity profile in the calculations, when actually the intensity distribution has a Bessel function dependence; we find the total calculated flux dependence on intensity and detuning to be insensitive to the exact distribution of the optical field. Furthermore, we ignore quantum tunneling to the wall and attractive van der Waals forces which are important at small atom-wall distances. Finally, we ignore the fact that the mode intensity decays along the z axis, which is valid for the short fibers used in the current experiments.

Starting with the first assumption, the atoms at the input cross section of the fiber have the normalized velocity distribution

$$f(\mathbf{u}_\perp,u_z)=\pi^{-3/2}(\nu_\perp/\nu_T)^2\exp[-u_z^2-(\nu_\perp/\nu_T)^2u_\perp^2] \quad (5)$$

and are uniformly distributed in space. The total flux striking the hole in the fiber is then given by

$$J_i=\int_{x_0^2+y_0^2<1}dx_0dy_0\int_{u_z>0}du_z\int d\mathbf{u}_\perp u_z f(\mathbf{u}_\perp,u_z)=\tfrac{1}{2}\sqrt{\pi}. \quad (6)$$

(This flux is dimensionless, the physically measured flux given as atoms per unit time is $\mathcal{F}_i=J_i\nu_T/l$.) Of the atoms entering the fiber, only those that do not strike the wall emerge at the output end. The atoms that hit the wall we assume are lost from the guide. Thus, in the absence of an optical guiding potential, the atoms must follow a ballistic trajectory through the fiber, and the flux emerging from the fiber is simply the input flux multiplied by the solid angle subtended by the fiber output $J_0=J_i(r_c/l)^2$.

In the presence of the optical field the transverse atomic motion is bound by the optical potential. The corresponding output flux

$$J(\Delta_n)=\int_{x_0^2+y_0^2<1} dx_0 dy_0 \int_{u_2>0} du_z \int_s d\mathbf{u}_\perp u_z f(\mathbf{u}_\perp, u_z) \tag{7}$$

is calculated by integrating over the velocity region S containing atoms passing through the fiber ballistically, and those that undergo at least one bounce. To obtain a considerable increase in the atomic flux due to the presence of the optical field, the latter contribution should be considerably larger, so in the following we neglect the contribution from ballistic atoms. Thus the results obtained below are valid for $J(\Delta_n)>J_0$.

Assuming a straight piece of fiber and excitation of only the lowest-order, azimuthally symmetric light mode, the potential is cylindrically symmetric, and angular momentum is conserved. This momentum conservation may be expressed as $M=u_\phi\rho=$const, where u_ϕ is the azimuthal component of the atom's velocity, and $\rho=(x^2+y^2)^{1/2}$ is the magnitude of the radial coordinate. Integration of Eq. (4c) then gives

$$u_\rho^2+\frac{M^2}{\rho^2}-\delta\ln\left(1+\frac{I(\rho)}{2\delta^2}\right)=E, \tag{8}$$

where E is the total center-of-mass transverse energy, kinetic plus potential, of the atom.

The region of parameters corresponding to the trapped atoms S is determined from the condition that the energy of an atom entering the fiber at the point (ρ,ϕ) with the velocity components (u_ρ,u_ϕ) is less than the minimum energy $E_{\min}=M^2+\delta\ln[1+I(\rho=1)/2\delta^2]=M^2$ of an atom with the same value of the angular momentum M at the wall [recall that $I(\rho=1)=0$]. This condition can be expressed as

$$S=\left\{\rho,\phi,u_\rho,u_\phi : u_\rho^2+(1-\rho^2)u_\phi^2<\delta\ln\left(1+\frac{I(\rho)}{2\delta^2}\right)\right\}. \tag{9}$$

Integrating Eq. (7) with condition (9) over the transverse components of the velocity and the azimuthal angle ϕ, one finds

$$J(\Delta_n)=2a^2J_0\int_0^1\frac{d\rho^2}{\sqrt{1-\rho^2}}\int_\zeta^\infty du_z u_z\exp(-u_z^2)\times\delta\ln\left(1+\frac{I(\rho)}{2\delta^2}\right), \tag{10}$$

where $\zeta=\max(0,\Delta_n/s)$. The spatial integral in Eq. (10) requires that the intensity profile, or more specifically, the optical potential, be specified. We take the optical potential to be a box in order to obtain analytic results. For the box potential,

$$J(\Delta_n)=4a^2J_0\int_\zeta^\infty du_z u_z\exp(-u_z^2)\,\delta\ln\left(1+\frac{1}{2\delta^2}\right). \tag{11}$$

We have also evaluated Eq. (10) with a parabolic intensity distribution, and found that the flux detuning dependence is very similar to Eq. (11) but is roughly 2–3 times smaller. Thus we conclude that the flux profile is largely independent of the exact shape of the potential in the low intensity limit.

In general the equation must be solved numerically, but one can obtain an analytic reduction of the integral in Eq. (11) in a few limiting cases. There are three frequencies that characterize our problem: the detuning Δ, the Doppler frequency $k\nu_T$, and the Rabi frequency ω_R. Recall that these three frequencies are imbedded in the two dimensionless quantities $\Delta_n=\Delta/\omega_R$ and $s=k\nu_T/\omega_R$. The relative sizes of these frequencies provide the various limiting cases of interest. For example, for detunings large compared to the Doppler width, $|\Delta_n|\gg s$, ζ can be set equal to 0 and δ can be treated as independent of u_z, reducing Eq. (11) to the expression

$$J(\Delta_n<0)\approx 2J_0\left(\frac{l}{r_c}\right)^2\frac{\hbar\omega_R}{m\nu_T^2}|\Delta_n|\ln\left(1+\frac{1}{2\Delta_n^2}\right). \tag{12}$$

If we additionally assume that the detuning is much larger than the Rabi frequency, $|\Delta_n|\gg 1$, the flux given by Eq. (12) becomes

$$J(\Delta_n<0)\approx J_0\left(\frac{l}{r_c}\right)^2\frac{\hbar\omega_R^2}{|\Delta_n|m\nu_T^2}=J_i\frac{\hbar}{m\nu_T^2}\frac{\omega_R^2}{|\Delta_n|}, \tag{13}$$

which is proportional to the intensity and inversely proportional to the detuning. The condition of applicability of Eq. (12) $|\Delta_n|\gg s$ also implies $|\Delta_n|\gg 1$, so this is the only case possible for small intensities. On the other hand, for large intensities the condition $|\Delta_n|\gg s$ can hold for both $|\Delta_n|\gg 1$ and $|\Delta_n|\ll 1$; the flux expressed in relation (12) as a function of the frequency detuning passes through a maximum for $|\Delta_n|\approx 0.35$.

In the limit of small negative or positive detunings $|\Delta_n|\ll s$ and for small intensities such that $\omega_R\ll k\nu_T$, the flux is approximately given by the relation

$$J(\Delta_n=0)\approx J_0\left(\frac{l}{r_c}\right)^2\frac{\hbar\omega_R^2}{km\nu_T^3}=J_i\frac{\hbar}{m\nu_T^2}\frac{\omega_R^2}{k\nu_T}, \tag{14}$$

whereas for large intensities, such that $\omega_R\gg k\nu_T$, its value is

$$J(\Delta_n=0)\approx J_0\left(\frac{l}{r_c}\right)^2\frac{k\hbar}{m\nu_T}\ln\frac{\omega_R^2}{2k^2\nu_T^2}=J_i\frac{\hbar}{m\nu_T^2}k\nu_T\ln\frac{\omega_R^2}{2k_2\nu_T^2}. \tag{15}$$

For all of the intermediate cases, the final integral over longitudinal velocities must be performed numerically. We defer a discussion of the results of these numerical calculations to Sec. V, where we compare them to experimental measurements.

C. Conservative limit, curved fibers

Consider now the situation when the fiber is bent in the (Y,Z) plane with a radius of curvature R. Some atoms are lost from the guide when their relatively large axial velocity is converted into transverse velocity, and the potential is insufficient to contain the atoms. In an alternative picture, atoms traversing a bent fiber experience a centrifugal force which presses them into the outer wall of the fiber, and they

are lost when the guide potential exerts insufficient force to overcome the centrifugal force. The following calculation of flux through a curved fiber is similar to the calculation in Sec. IV B, but with an additional energy contribution from the centrifugal potential.

For the bent fiber, instead of the initial coordinates (X,Y,Z), we introduce a curvilinear system of coordinates (X',Y',Z'), with the axis Z' following the bent fiber

$$X=X', \tag{16a}$$

$$Y=R[1-\cos(Z'/R)]+Y'\cos(Z'/R), \tag{16b}$$

$$Z=(R-Y')\sin(Z'/R). \tag{16c}$$

The unit vectors $(\mathbf{e}_{x'},\mathbf{e}_{Y'},\mathbf{e}_{z'})$ for this coordinate system are related to the old set $(\mathbf{e}_x,\mathbf{e}_Y,\mathbf{e}_z)$ by the expressions

$$\mathbf{e}_{x'}=\mathbf{e}_x, \tag{17a}$$

$$\mathbf{e}_{Y'}=\mathbf{e}_Y\cos(Z'/R)-\mathbf{e}_Z\sin(Z'/R), \tag{17b}$$

$$\mathbf{e}_{Z'}=\mathbf{e}_Y\sin(Z'/R)+\mathbf{e}_Z\cos(Z'/R), \tag{17c}$$

and the components of velocity by the expressions

$$\nu_{X'}=\nu_X, \tag{18a}$$

$$\nu_{Y'}=\nu_Y\cos(Z'/R)-\nu_Z\sin(Z'/R), \tag{18b}$$

$$\nu_{Z'}=\nu_Y\sin(Z'/R)+\nu_Z\cos(Z'/R). \tag{18c}$$

As in Sec. IV B, we introduce the dimensionless coordinates and velocities determined by the relations $(x,y,z)=(X'/r_c,Y'/r_c,Z'/l)$, $(u_x,u_y,u_z)=(\nu_x,/\nu_\perp,\nu_y/\nu_\perp,\nu_z/\nu_T)$.

In these dimensionless coordinates, Eq. (4) takes the forms

$$\frac{dz}{d\tau}=u_z, \tag{19a}$$

$$\frac{d\boldsymbol{\rho}_\perp}{d\tau}=a\mathbf{u}_\perp, \tag{19b}$$

$$\frac{d\mathbf{u}_\perp}{d\tau}=\frac{a\delta}{2}\left(\frac{I}{I+2\delta^2}\right)\frac{\boldsymbol{\nabla}_\perp I}{I}+\frac{b\delta}{2}\left(\frac{I}{I+2\delta^2}\right)^3\left(\mathbf{u}_\perp\cdot\frac{\boldsymbol{\nabla}_\perp I}{I}\right)\frac{\boldsymbol{\nabla}_\perp I}{I}-\mathbf{e}_y a\left(\frac{\nu_T}{\nu_\perp}\right)^2\frac{r_c}{R}u_z^2, \tag{19c}$$

where $\mathbf{e}_y$ is the unit vector in the direction of the new y coordinate. Direct comparison of Eq. (19) with Eq. (4) shows that, for a bent fiber, the equations of motion acquire an additional centripetal force term.

The region of the input velocities and the coordinates corresponding to the trapped atoms determined by conservation of energy is $u_x^2+u_y^2<\delta\ln(1+1/2\delta^2)$. If we assume, for simplicity, that the cross section of a fiber is a square $-1<x<1$, $-1<y<1$, then the x and y velocity components separate and the trapping condition for the x coordinate is

$$u_x^2<\delta\ln\left(1+\frac{1}{2\delta^2}\right). \tag{20}$$

Note that this trapping condition may be evaluated at either the lower $(x=-1)$ or the upper $(x=1)$ boundaries of the fiber since they are identical.

The motion of an atom along the y coordinate according to Eq. (19) is analogous to the motion of a particle in a gravity field with the effective acceleration constant $g=(\nu_T/\nu_\perp)^2(r_c/R)u_z^2$, which implies the energy conservation law of the form $u_y^2+2(\nu_T/\nu_\perp)^2(r_c/R)u_z^2y=\text{const}$. The trapping condition for this coordinate should be estimated at the lower (physically the outer) boundary of the fiber $y=-1$ and read

$$u_y^2+2\left(\frac{\nu_T}{\nu_\perp}\right)^2\frac{r_c}{R}u_z^2(y_0+1)<\delta\ln\left(1+\frac{1}{2\delta^2}\right). \tag{21}$$

The particle flux is calculated as in Sec. IV B using a flat-topped intensity distribution. Carrying out integration over the transverse components of velocity (u_x,u_y) and the transverse cross section of the fiber (x_0,y_0) and accounting for the limits in Eqs. (20) and (21), one finds

$$J(\Delta_n)=2a^2J_0\int_\zeta^\infty du_z u_z\exp(-u_z^2)\,\delta\ln\left(1+\frac{1}{2\delta^2}\right)\Phi(\kappa), \tag{22}$$

where in this case $\zeta=\max(0,\Delta_n/s)$ and $J_0=8\pi^{-3/2}(r_c/l)^2=4\pi^{-1}(r_c/l)^2J_i$. The effective reduction of the flux due to the bending of the fiber is described by the function $\Phi(\kappa)$ determined by the relations

$$\Phi(\kappa)=\begin{cases}\dfrac{2}{3\kappa}\left[1-(1-\kappa)^{3/2}\right], & \kappa<1\\[2ex] \dfrac{2}{3\kappa}, & \kappa>1,\end{cases} \tag{23}$$

where

$$\kappa=4\left(\frac{\nu_T}{\nu_\perp}\right)^2\frac{r_c}{R}\frac{u_z^2}{\delta\ln(1+1/2\delta^2)}. \tag{24}$$

Note that Eq. (22) in the limit $R\to\infty$ is similar to Eq. (11), but differs by a factor of 2 and includes the function Φ in the integrand. Note also that the relative degree of the flux reduction due to the bending of the fiber, and governed by the function Φ, is independent of the fiber length. A physical reason for this is that the main bulk of the flux is carried by atoms experiencing many bounces between the walls of the potential well. If an atom survives a couple of bounces it will remain trapped through the rest of the fiber. The effective reduction parameter κ is directly related to the angular change of the fiber's axis between two successive bounces of the atom.

For negative detunings such that $|\Delta_n|\gg s$, Eq. (22) reduces to the expression

$$J(\Delta_n<0)=J_0a^2|\Delta_n|\ln\left(1+\frac{1}{2\Delta_n^2}\right)\int_0^\infty dx\,\exp(-x)\Phi(\alpha x), \tag{25}$$

where

$$\alpha=4\left(\frac{\nu_T}{\nu_\perp}\right)^2\frac{r_c}{R}\frac{1}{|\Delta_n|\ln\left(1+\frac{1}{2\Delta_n^2}\right)}. \tag{26}$$

In the limit of a large bend radius, $\alpha\ll 1$, and Eq. (25) recovers the straight-fiber result of Sec. II A given by Eq. (12),

$$J(\Delta_n<0)=J_0\left(\frac{l}{r_c}\right)^2\frac{\hbar\omega_R}{m\nu_T^2}|\Delta_n|\ln\left(1+\frac{1}{2\Delta_n^2}\right). \tag{27}$$

For $\alpha\gg 1$, Eq. (25) yields

$$J(\Delta_n<0)=\frac{2J_0}{3}a^2|\Delta_n|\ln\left(1+\frac{1}{2\Delta_n^2}\right)\frac{1}{\alpha}\ln\alpha. \tag{28}$$

In the small-intensity limit when $|\Delta_n|\gg 1$, this further reduces to

$$J(\Delta_n<0)=\frac{2J_0}{3}\left(\frac{\hbar\omega_R}{4m\nu_T^2|\Delta_n|}\right)^2\frac{l^2R}{r_c^3}\ln\left(\frac{8m\nu_T^2|\Delta_n|r_c}{\hbar\omega_R R}\right). \tag{29}$$

The flux in this limit is less than that given by Eq. (13), proportional to the intensity squared and inversely proportional to the detuning squared.

For near-zero detunings and small intensities where $\omega_R\ll k\nu_T$, the degree of the reduction in the flux due to the fiber bend is governed by the parameter $\beta=8(km\nu_T^3\hbar\omega_R^2)(r_c/R)$. For $\beta\ll 1$ (large R), the straight fiber result

$$J(\Delta_n=0)=\frac{\sqrt{\pi}J_0}{4}\frac{\hbar\omega_R^2}{km\nu_T^3}\left(\frac{l}{r_c}\right)^2=\frac{J_0}{\sqrt{\pi}}\frac{\hbar\omega_R^2}{km\nu_T^3} \tag{30}$$

is recovered, differing from Eq. (14) only by a numerical coefficient of the order of unity.

Decreasing the radius of the bend decreases the flux. In the opposite limit, for $\beta\gg 1$ and $\beta^{1/3}\ll k\nu_T/\omega_R$, Eq. (22) reduces to

$$\begin{aligned}J(\Delta_n=0)&=\frac{J_0}{2}\left(\frac{\hbar\omega_R^2}{km\nu_T^3}\right)^{4/3}\left(\frac{l}{r_c}\right)^2\left(\frac{R}{r_c}\right)^{1/3}\\&=\frac{2J_i}{\pi}\left(\frac{\hbar\omega_R^2}{km\nu_T^3}\right)^{4/3}\left(\frac{R}{r_c}\right)^{1/3},\end{aligned} \tag{31}$$

which shows that the flux is less sensitive to fiber bending at zero detuning than at large detunings [Eq. (29)]. Also, the functional dependence on the intensity becomes $I^{4/3}$ instead of I, as in the case of straight fiber [Eq. (30)]. The dependence of the flux on the radius of the bend R is also milder than for Eq. (29). For large intensities $\omega_R\gg k\nu_T$ the parameter β controlling the degree of the reduction in the flux due to the bending of the fiber is of the form $\beta=4(m\nu_T/\hbar k)(r_c/R)\ln^{-1}(\omega_R^2/2k^2\nu_T^2)$.

The limit of small β recovers the high-intensity straight fiber limit given by Eq. (15). In the opposite limit, $\beta\gg 1$ Eq. (25) yields a lower flux,

$$\begin{aligned}J(\Delta_n=0)&=J_0\left(\frac{\hbar k}{2m\nu_T}\right)^2\ln^2\left(\frac{\omega_R^2}{2k^2\nu_T^2}\right)\frac{l^2R}{r_c^3}\\&=J_{tot}\left(\frac{\hbar k}{2m\nu_T}\right)^2\ln^2\left(\frac{\omega_R^2}{2k^2\nu_T^2}\right)\frac{R}{r_c}.\end{aligned} \tag{32}$$

It is clear from Eq. (29) that in the large detuning limit the flux is proportional to the laser intensity squared, and inversely proportional to the detuning squared. This result is particularly interesting in regards to the coherent transport of atoms through curved fibers. In order to reduce spontaneous emission and hence the loss of coherence, it is necessary to detune the laser far from resonance. However, in curved fibers the guiding potential falls off at the same rate as spontaneous emission, as Δ^{-2}. Thus the reduction in spontaneous emission comes at the expense of a proportional reduction in guide potential.

D. Nonconservative limit, straight fibers

In the presence of the nonconservative viscous term in the equations of motion, the energy of an atom depends on the distance traveled inside the fiber. For negative detunings this term results in an increase of the transverse energy of the atom with the longitudinal coordinate (heating). The amount of this change can be calculated by multiplying Eq. (3b) by $u_\perp$, and integrating from $\tau=0$ to $\tau=1/u_z$. The conservative term does not heat the atoms, since it depends only on the transverse position of the atom and can be neglected. Taking simple approximations for the second term, $l\approx 1$ and $\nabla I/I\approx 1$, and averaging over the period of one transverse oscillation we relate the average radial kinetic energy of the atom at the fiber output to its initial radial kinetic energy,

$$u_\rho^2=u_\rho^2(0)\exp\left[\frac{b}{u_z}\,\delta\left(\frac{1}{1+2\delta^2}\right)^3\right]. \tag{33}$$

This shows that the transverse energy increases exponentially as a function of distance along the fiber. The flux is calculated as in Sec. IV B, except that the guiding condition should be estimated at the output of the fiber where the radial transverse component of the atom velocity is the largest. Equation (11) is then replaced in the high-intensity limit by the expression

$$\begin{aligned}J(\Delta_n)=a^2J_0\int_\zeta^\infty du_z u_z\exp(-u_z^2)\,\delta\ln\left(1+\frac{1}{2\delta^2}\right)\\\times\exp\left[-\frac{b\delta}{u_z}\left(\frac{1}{1+2\delta^2}\right)^3\right].\end{aligned} \tag{34}$$

In general this integral must be performed numerically. The numerical results are presented in Sec. V and compared with experimental measurements.

Some asymptotic limits can be solved analytically. For near-zero detunings, Eq. (34) reduces to

$$J(\Delta_n=0)\approx J_0\left(\frac{l}{r_c}\right)\frac{\hbar k}{m\nu_T}\int_0^\infty du_z u_z^2\exp(-u_z^2)\times\ln\left(1+\frac{1}{2s^2u_z^2}\right)\exp[-bs(1+2s^2u_z^2)^{-3}]. \tag{35}$$

In the low-intensity limit $\omega_R \ll k\nu_T$, the degree of the reduction of the flux is governed by the parameter $\alpha=(3l\hbar k/8mr_c^2\Gamma)^{1/4}(\omega_R/k\nu_T)^{3/2}$, and Eq. (35) yields

$$J(\Delta_n=0)=J_i\frac{\hbar\omega_R^2}{mk\nu_T^3}\exp\left[-\frac{4}{3}\alpha\right]=J_i\frac{\hbar\omega_R^2}{mk\nu_T^3}\exp\left[-\frac{4}{3}\left(\frac{3l\hbar k}{8mr_c^2\Gamma}\right)^{1/4}\left(\frac{\omega_R}{k\nu_T}\right)^{3/2}\right]. \tag{36}$$

Comparison with Eq. (14) shows that the flux for zero detuning in the low-intensity limit decreases exponentially with the optical intensity as $\exp(\alpha I^{3/4})$. In the opposite limit of large intensities $\omega_R \gg k\nu_T$, Eq. (35) results in the expression

$$J(\Delta_n=0)=J_i\frac{\hbar k}{m\nu_T}\ln\left(\frac{\omega_R^2}{2k^2\nu_T^2}\right)\exp\left(-\frac{l\hbar k}{mr_c\Gamma}\right). \tag{37}$$

The flux reduction due to heating now is independent of intensity, and is given by the reduction parameter $\exp(-l\hbar k/mr_c^2\Gamma)$ [compare with Eq. (15)].

For large negative detunings $|\Delta_n| \ll s$, the flux reduction parameter equals

$$\alpha=\left(\frac{l\hbar\omega_R}{2mr_c^2\Gamma\nu_T}\right)^{2/3}\frac{|\Delta_n|^{2/3}}{(1+2\Delta_n^2)^2}. \tag{38}$$

The limit $\alpha \ll 1$ recovers the conservative-case results given by Eq. (12). In the opposite limit, $\alpha \gg 1$, but still $s\sqrt{\alpha} \ll 1$ Eq. (34) yields

$$J(\Delta_n<0)=J_i\frac{\hbar\omega_R}{m\nu_T^2}|\Delta_n|\ln\left(1+\frac{1}{2\Delta_n^2}\right)\sqrt{\alpha}\exp(-3\alpha). \tag{39}$$

For the detunings exceeding the Rabi frequency $|\Delta_n| \gg 1$, Eq. (39) can be further transformed to the form

$$J(\Delta_n<0)\approx J_i\left(\frac{\hbar\omega_R}{m\nu_T^2}\right)^{4/3}\left(\frac{l\nu_T}{r_c^2\Gamma}\right)^{1/3}\Delta_n^{-8/3}\times\exp\left[-\frac{3}{4}\Delta_n^{-10/3}\left(\frac{l\hbar\omega_R}{2mr_c^2\Gamma\nu_T}\right)^{2/3}\right]. \tag{40}$$

V. COMPARISON OF THEORY AND EXPERIMENT

Section IV assembled a collection of formulas for the calculation of atom flux through the hollow core fiber. We have modeled the major regimes covered by experimental measurements except for the case of the curved fiber with large guide intensities. In the curved fiber case the flux acquires a much greater dependence on the shape of the optical field. Curvature of the fiber in fact alters the optical field distribution from the unperturbed, lowest-order grazing incidence mode. This, along with the fact that the optical field decays exponentially along the length of the fiber, makes quantitative modeling difficult. Nevertheless, as we show in this section, we can describe the qualitative behavior of the flux through the fiber reasonably well in all cases.

In Fig. 2 we presented measurements of the flux dependence on detuning from resonance for a straight fiber with an inner diameter of 40 μm. For data of Fig. 2(a), the fiber length is 3.1 cm and a single-mode, 5-mW diode laser provides the guiding potential. At large negative detunings the flux falls off as $1/\Delta$, and is sharply peaked near zero detuning. This data are representative of the low-intensity regime, and the excellent signal-to-noise ratio allows a direct comparison with Eq. (10), represented by the solid curve. The numerical calculation was performed using a parabolic intensity profile. With no laser or with the laser detuned far to the blue of resonance, $\Delta \geqslant 40$ GHz, the detector counts come from two sources: from atoms passing ballistically through the fiber and from detector noise of approximately ten counts per second. For intermediate blue detunings, $\Delta \approx 3$–30 GHz, a dip down to the detector background count rate is observed. This dip, four atoms per second in amplitude [not noticeable in Fig. 2(a)], is attributed to the loss of ballistic flux as these atoms are deflected into the wall of the fiber by the repulsive dipole force. The ratio of the peak guided atom flux to ballistic flux is then easily compared to theory. We observed an enhancement factor of $800/4=200$ which is in agreement with the 200-fold enhancement predicted from Eq. (10) with the parabolic intensity distribution and a peak Rabi frequency measured at the output tip of the fiber. We note that no adjustable parameter is used for the theory curve of Fig. 2(a). We also note that qualitatively the flux profile is narrower than a dispersion line shape. This is because the flux is proportional to the dipole *potential*, $(\hbar\delta/2)\ln(1+\omega_r/\delta)$, and not the dipole *force* which is dispersion shaped.

The position of maximum flux occurs at a detuning of ~ 1 GHz, roughly corresponding to the value of $0.35\omega_R=1.5$ GHz predicted in Sec. IV B. With a good signal-to-noise ratio and small intensities, a small peak near $\Delta=+1.5$ GHz is observed. This peak is due to the hyperfine splitting of the $5S_{1/2}$ ground state of rubidium. At small intensities the shift of the ground state due to the dynamic stark effect is much less than the hyperfine splitting (3.0 GHz), and the dipole force may be described by two dispersion lineshapes separated by 3.0 Ghz. The peak at $\Delta=+1.5$ GHz is smaller because of optical pumping of atoms out of the guided state and into the nonguided state. To confirm this explanation we have performed a separate experiment in which we fixed the guide laser at $\Delta=0$ and then tuned a second, weaker laser over the hyperfine resonances. We found that when the second laser excited atoms on the reddest hyperfine transition ($\omega > \omega_L$), atoms would be optically pumped into the bluer state ($\omega > \omega_L$) and guided through the fiber. However, when the laser is tuned to the bluer hyperfine transition, atoms are pumped into the red state (so that effectively the laser is blue detuned relative to the atoms) and guiding is inhibited. At high intensities the individual dipole force dispersion profiles

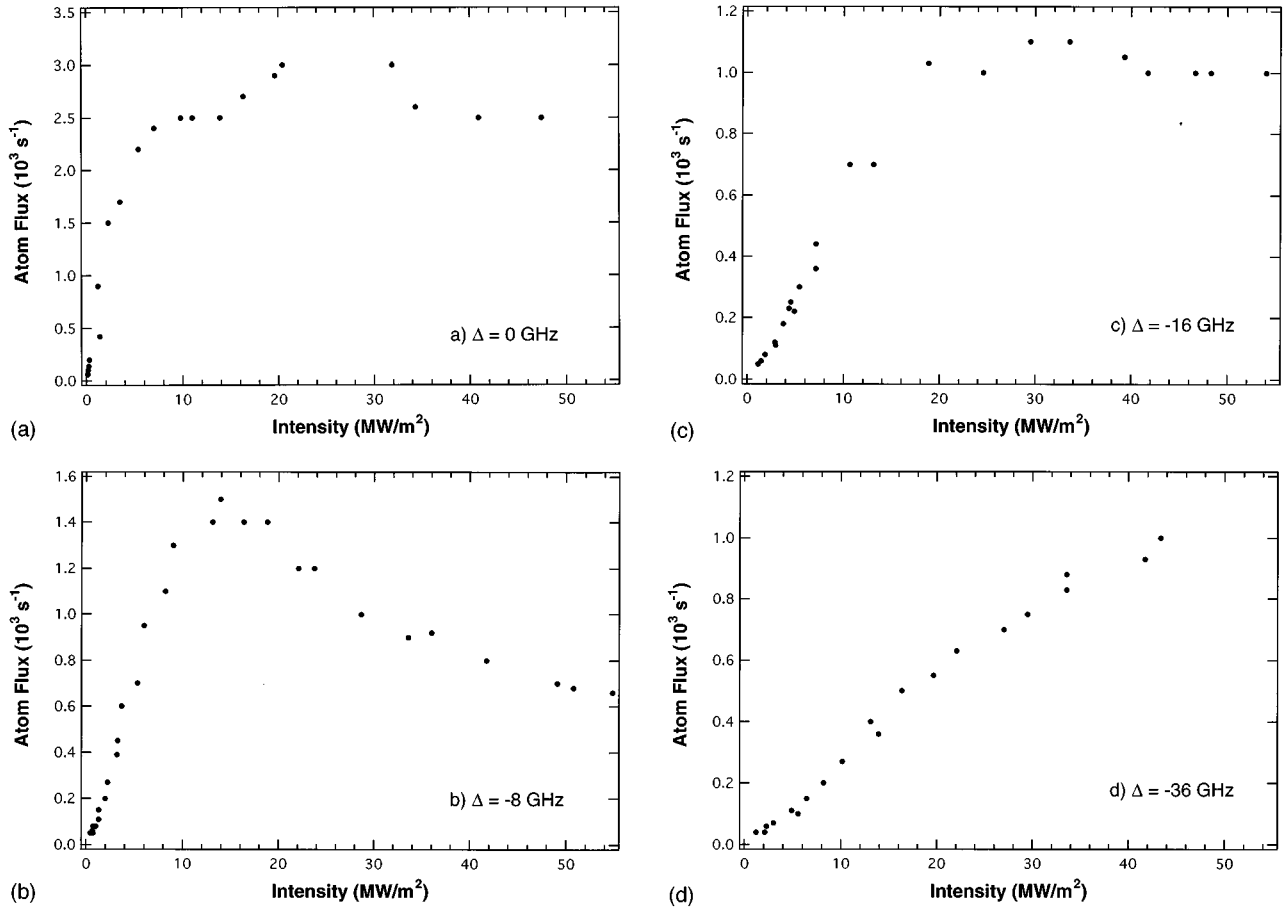

FIG. 5. Measurements of the intensity dependence of the guided atom flux in a 6.2-cm-long fiber at (a) $\Delta=0$, (b) -8, (c) -16, and (d) $\Delta=-36$ GHz. At small intensities where the heating effects are negligible the flux grows linearly with intensity for all detunings. At higher intensities and at intermediate detunings, $\Delta=-8$ GHz, the flux rools over and decreases. This behavior indicates that dipole heating attenuates the flux through the fiber. For large detunings the flux is described by the conservative limit of linear intensity dependence up to the experimental intensities available. The profiles here are in good qualitative agreement with calculations shown in Fig. 6.

are indistinguishable and the peak at $\Delta=+1.5$ GHz is not observed.

In Figs. 2(b)–2(d), measured and calculated flux profiles are presented with successively increasing intensities. The single-peaked spectrum of the low-intensity regime clearly splits into two peaks: one sharp centered near-zero detuning and one broad extending to large negative frequencies. At larger intensities the dip grows wider and deeper. Superimposed on the data are numerical results from calculations of Eq. (34). For the calculation the Rabi frequency is reduced to half of the measured value and the curves are normalized to the data. The Rabi frequency is reduced to account for the use of a flattop radial intensity profile in contrast to the more accurate, parabolic profile used in Fig. 2(a). Qualitatively, the shape of the curve can be explained by velocity dependent forces which heat the atoms: at intermediate frequencies where the heating force is largest, atoms are heated out of the guide potential and lost. For large frequencies, however, the heating force falls off faster (as Δ^{-5}) than the conservative guiding force (as Δ^{-1}), thus allowing more atoms to be guided and explaining the origin of the second peak. At larger detunings the heating force is negligible and the profile is described by the conservative force alone. As a result the flux falls off as Δ^{-1} for large detunings. The spike near zero detuning is similarly understood in terms of the heating force decreasing faster than the guiding force as $\Delta\rightarrow 0$.

We note that the theoretical fit to the experimental data is qualitative, a consequence one may expect from the averaging process used to obtain Eq. (34). In addition we have made no correction for the fact that the light attenuates by a factor of $\sim e^{-2}$ over the fiber length. However, the calculations do reproduce the features observed in the data quite well, and they confirm the dipole force heating explanation of the observed dip in the experimental profile.

In Figs. 5(a)–5(d) we show measurements of the flux intensity dependence at selected detunings. At low intensities the flux grows linearly with intensity regardless of detuning. This is expected since the heating force is not significant at low intensities, and the flux is described by the conservative force alone. Nonlinearities in the flux are evident at larger intensities. For $\Delta=0$ the flux begins to saturate at $I=5\text{MW/m}^2$, and reaches an asymptotic limit at higher intensities. For $\Delta=-8$ GHz the flux also saturates, near $I=5\text{MW/m}^2$, but instead of approaching an asymptotic limit it decreases. This behavior indicates that the heating rate grows faster than the guiding potential, and atoms are lost as they are heated to energies larger than the depth of the guiding potential. At $\Delta=-16$ GHz, evidence of heating is observed at higher intensities. We see no evidence of heating at $\Delta=-36$ GHz for the available experimental intensities.

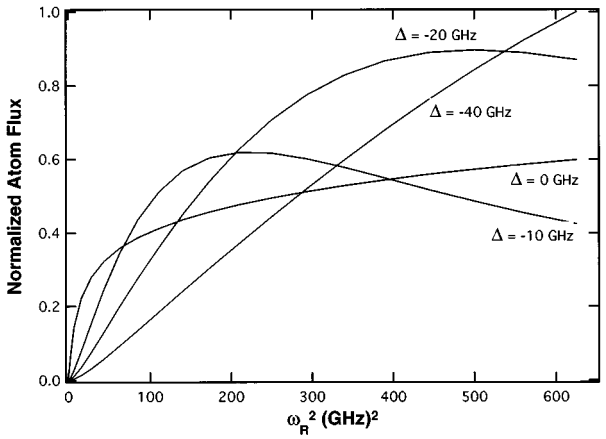

FIG. 6. Calculations of the dependence of guided atom flux on intensity, indicated in terms of the squared Rabi frequency ω_R^2, for the indicated detunings from resonance. The calculations are based on a numerical evaluation of Eq. (34) and assume a flat top radial intensity distribution. The horizontal scale and detunings roughly correspond to the experimental parameters of Fig. 5. Heating effects observed in the experimental measurements are clearly manifest in the calculations as well and the qualitative agreement is good.

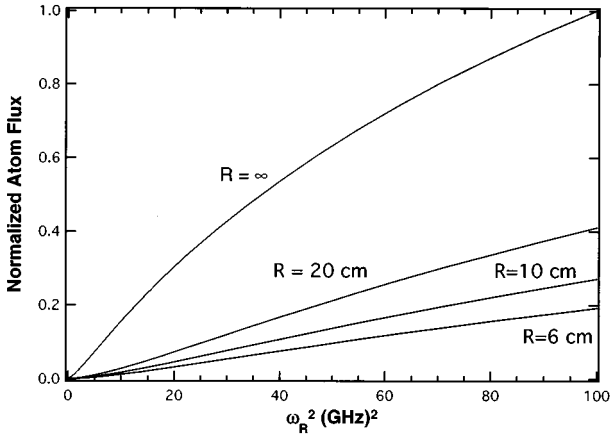

FIG. 7. Numerical calculations of the atom flux dependence on intensity indicated as ω_R^2 in the conservative regime for fibers with several radii of curvature. The parameters are $\Delta=-3$ GHz, $l=6$ cm, $r_c=10$ μm, and $k\nu_T=2$ GHz. For perfectly straight fibers the flux depends linearly on intensity initially, and then increases as a logarithm at large intensity. In curved fibers the flux initially increases as intensity is squared, and at larger intensities it has a logarithmic dependence. These calculations are in good qualitative agreement with data presented in Ref. [1].

In Fig. 6 we show calculations of the dependence of guided atom flux on intensity (indicated as ω_R^2) for the indicated detunings from resonance. The calculations are based on a numerical evaluation of Eq. (34), assuming a flattop radial intensity distribution. The horizontal scale and detunings roughly correspond to the experimental parameters of Fig. 5. Heating effects observed in the experimental measurements are clearly manifest in the calculations, and the qualitative agreement is good. In particular the saturation of the flux for $\Delta=0$ is in good agreement with Eq. (34) and the asymptotic form Eq. (27), which states that the flux at $\Delta=0$ depends only on the length of the fiber and is independent of laser intensity at high intensities. Decreasing flux is also predicted at intermediate detunings, and for large detunings the flux increases linearly with intensity.

Atom guiding in curved fibers is more complicated because of the additional centrifugal force acting to push the atoms into the outer wall. In the simplest picture, approximately valid in the low-intensity regime, the centrifugal force, $F_c=m\nu_z^2/R$ predominantly affects atoms with large longitudinal velocities as discussed in Sec. IV. As a result, the high-velocity tail of the Maxwell-Boltzmann distribution is lost first as the fiber is bent. Thus, as a function of $1/R$, we expect the flux to decrease monotonically to zero. The intensity dependence of the curved fiber flux is a complicated function of bend radius, detuning, and heating effects. The low-intensity regime where heating effects are minimal is the simplest to describe, and is reached by reducing the laser intensity or the fiber length. In Fig. 7 we present calculations of the dependence of guided atom flux on intensity for several fiber radii of curvature. The calculations have the expected dependence that the flux monotonically decreases as the fiber is bent to smaller radii. The intensity dependence of the straight fiber case, $R=\infty$, increases linearly from zero, and eventually begins to saturate as a logarithm at large intensity. In curved fibers and at small intensities the flux increases as the square of intensity, reflecting the fact that only the low-velocity tail of the Maxwell distribution is guided around the bend. At high intensities the potential begins to saturate, and the flux intensity dependence is logarithmic. The calculations shown in Fig. 7 produce the same qualitative behavior as the curved fiber data presented in Ref. [1].

At similar intensities but with longer fibers, the heating force complicates the curved fiber description of atom guiding. In the absence of a model, we can nevertheless heuristically explain the dominant features of the experimental results. The centrifugal force arising from the curvature of the fiber presses the atomic beam toward the outer wall of the fiber and away from the center of the optical intensity distribution. This has several consequences. First, at large detunings from resonance, the additional centrifugal force effectively reduces the guiding potential height by pushing the atoms toward lower intensity at the wall. In particular, this effect contributes an additional attenuation factor of Δ^{-1} to the flux profile, as shown by Eq. (29), and is most pronounced at large detunings. At intermediate detunings, heating effects dominate, and the situation is different. Compressing the atomic beam against the outer wall, the average field intensity seen by the atom is reduced and consequently the heating force is reduced relative to the guiding force. Thus, for intermediate detunings, the guided atom flux may actually increase in slightly bent fibers due to the strong suppression of the heating force. We show measurements of the flux profiles in Fig. 8 that qualitatively substantiate this trend. For the straight fiber case in Fig. 8(a), we observe a typical two-peak spectrum with a hole burned between the peaks. For the moderately curved fiber cases shown in Figs. 8(b) and 8(c), the flux is attenuated strongly at large detunings due to the Δ^{-2} scaling, but at intermediate detunings the flux actually increases.

As mentioned above, we have not incorporated these effects into our current numerical model primarily because tractable solutions to the equations of motion in the bent

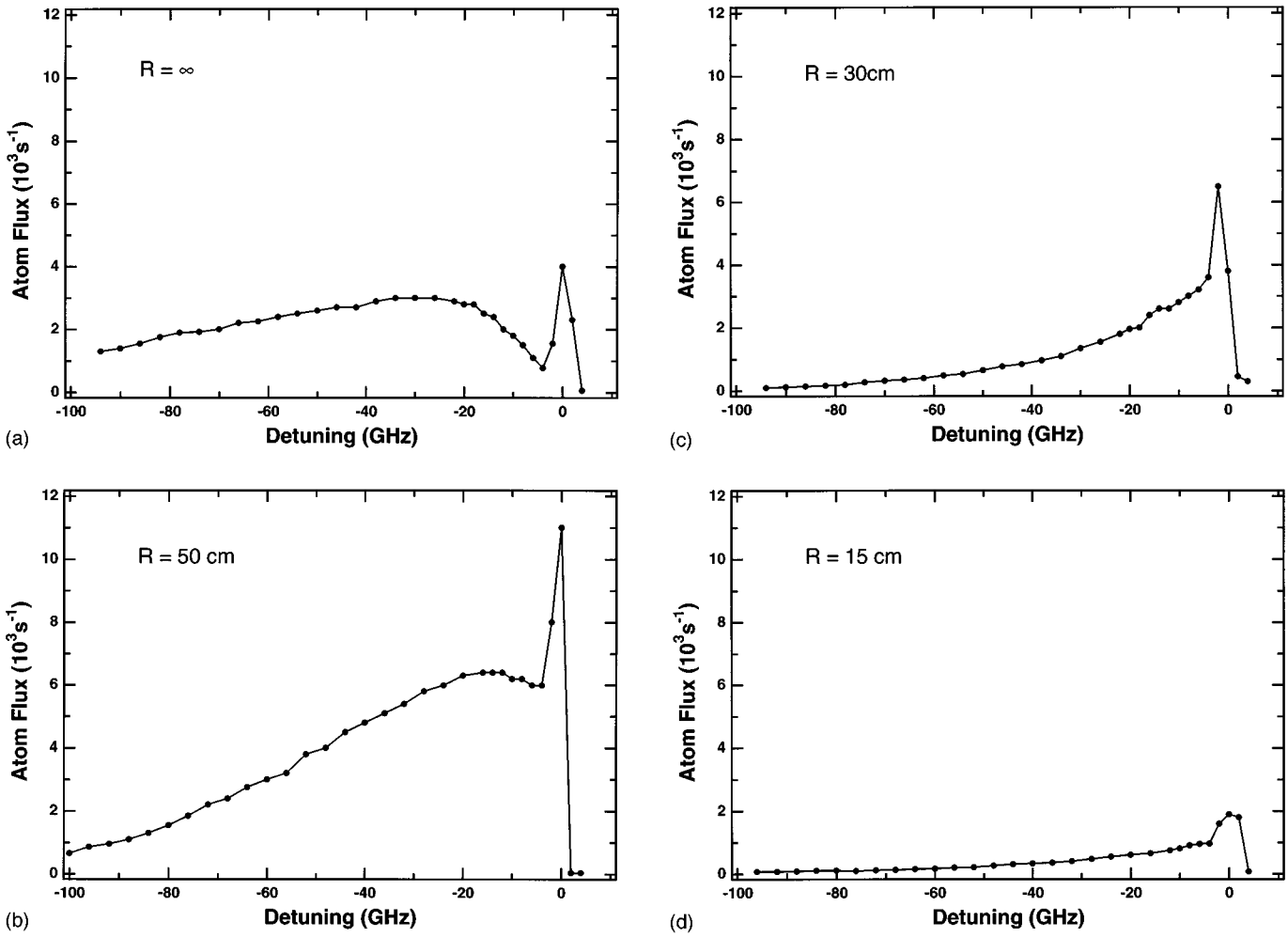

FIG. 8. Detuning profiles of flux in bent fibers at $I_0 = 1 \times 10^7$ W/m^2 and $l = 6.2$ cm. For the straight fiber case (a) the profile is clearly double peaked which is characteristic of the high-intensity regime. With moderate bending (b) and (c), strong attenuation of the flux is observed at large detunings, which is in agreement with Eq. (12). At small and intermediate detunings the flux initially increases with bending as indicated by the disappearance of the hole and increasing amplitude of the spike at $\Delta = 0$ GHz. This surprising behavior suggests that the heating force which causes hole burning in the spectrum is reduced more rapidly compared to the guiding force as the fiber is bent. Finally for large bends (d) the flux is strongly attenuated at all detunings.

fiber case were possible only for a flattop intensity profile. Atoms in the flattop intensity profile feel the same peak intensity regardless of fiber curvature, and consequently the heating rate is unaffected by bending the fiber. Finally, for small R we only observe the spike at $\Delta = 0$, and monotonic attenuation of the flux for increasing detunings. Figure 8(d) illustrates this behavior. In this limit the flux scales approximately as Δ^{-2}, as predicted from Eq. (29).

VI. CONCLUSION

We have observed atom guiding in a hollow-core, optical fiber, grazing-incidence mode configuration. Signatures of two intensity regimes have been identified. For low intensities and short fibers the detuning dependence of the flux is approximately dispersion shaped, as expected from the conservative part of the dipole potential. Also, in this regime the flux increases linearly with intensity for all detunings, as expected. At high intensities and in long fibers dipole heating of the atoms becomes significant, and a hole is burned into the flux spectrum. At these detunings the flux initially increases linearly with intensity, but then rolls over and decreases at large intensities. This behavior signifies the entrance to the high-intensity regime. The observed spectra and intensity dependencies are in excellent quantitative agreement with numerical evaluation of general dipole force equations of motion in the low-intensity regime, and in good qualitative agreement in the high-intensity regime.

Atom guiding in curved fibers is more complicated because of the centrifugal forces acting on the atoms. An additional loss of flux is most noticeable at large detunings, where the flux attenuates as R/Δ^2. The flux near zero detuning in the high-intensity regime initially goes up with increasing bend. This counterintuitive result is consistent with a more rapid falloff of the heating force relative to the guiding force when the fiber is bent. In short fibers, Ref. [1] demonstrated that, with sufficient intensity, atoms may be guided in short curved fibers with $R \approx 5$ cm. In long fibers dipole heating and exponential attenuation of the laser inten-

sity restrict the bend radii to more modest values of 20 cm or so.

It is interesting to speculate about the prospects of using nonconservative dipole forces to *cool* atoms in the fiber. The heating and guiding forces observed in the present experiment change sign when sign of the detuning from resonance changes. In particular, atoms are repelled from high-intensity regions and may be guided with a blue detuned evanescent field [2,3,5,12]. The nonconservative force for the blue detuned case becomes dissipative, and may provide a convenient mechanism for cooling atoms as they travel through the fiber.

ACKNOWLEDGMENTS

We gratefully acknowledge the support of the Office of Naval Research (Grant No. N00014-94-1-0375) and the National Science Foundation (Grant No. Phy-95-12150).

[1] M. J. Renn *et al.*, Phys. Rev. Lett. **75**, 3253 (1995).
[2] M. J. Renn *et al.*, Phys. Rev. A **53**, R648 (1996).
[3] H. Ito *et al.*, Phys. Rev. Lett. **76**, 4500 (1996).
[4] M. A. Ol'shanii, Y. B. Ovchinnikov, and V. S. Letokhov, Opt. Commun. **98**, 77 (1992).
[5] S. Marksteiner *et al.*, Phys. Rev. A **50**, 2680 (1994).
[6] H. G. Unger, Bell Syst. Tech. J. **36**, 1253 (1957).
[7] E. A. J. Marcatili and R. A. Schmeltzer, Bell Syst. Tech. J. **43**, 1783 (1964).
[8] T. Abel, J. Hirsch, and J. A. Harrington, Opt. Lett. **19**, 1034 (1994).
[9] S. Jackel *et al.*, Opt. Lett. **20**, 1086 (1995).
[10] J. Dalibard and C. Cohen-Tannoudji, J. Opt. Soc. Am. **2**, 1707 (1985).
[11] J. P. Gordon and A. Ashkin, Phys. Rev. A **21**, 1606 (1980).
[12] H. Ito *et al.*, Opt. Commun. **115**, 57 (1995).